Advances in Computational Mathematics (2024) 50:67
https://doi.org/10.1007/s10444-024-10160-5

An adaptive finite element DtN method for the acoustic-elastic interaction problem

Lei Lin[1] · **Junliang Lv**[1] · **Shuxin Li**[1]

Received: 20 June 2023 / Accepted: 12 June 2024 / Published online: 8 July 2024

Abstract

Consider the scattering of a time-harmonic acoustic incident wave by a bounded, penetrable and isotropic elastic solid, which is immersed in a homogeneous compressible air/fluid. By the Dirichlet-to-Neumann (DtN) operator, an exact transparent boundary condition is introduced and the model is formulated as a boundary value problem of acoustic-elastic interaction. Based on a duality argument technique, an a posteriori error estimate is derived for the finite element method with the truncated DtN boundary operator. The a posteriori error estimate consists of the finite element approximation error and the truncation error of the DtN boundary operator, where the latter decays exponentially with respect to the truncation parameter. An adaptive finite element algorithm is proposed for solving the acoustic-elastic interaction problem, where the truncation parameter is determined through the truncation error and the mesh elements for local refinements are chosen through the finite element discretization error. Numerical experiments are presented to demonstrate the effectiveness of the proposed method.

Keywords Acoustic-elastic interaction problem · Adaptive finite element method · Transparent boundary condition · A posteriori error estimate

Mathematics Subject Classification (2010) 65N12 · 65N15 · 65N30

Communicated by: Jon Wilkening

Junliang Lv and Shuxin Li contributed equally to this work.

✉ Junliang Lv
lvjl@jlu.edu.cn

Lei Lin
linleijlu@126.com

Shuxin Li
lshuxin99@163.com

[1] School of Mathematics, Jilin University, Qianjin Street, Changchun 130012, Jilin Province, China

1 Introduction

Direct and inverse scattering play important roles in science and engineering field [6, 9, 34, 54]. In the present paper, we consider the scattering of the time-harmonic acoustic wave by a bounded, penetrable and isotropic elastic solid, where the elastic obstacle is immersed in a homogeneous and compressible air/fluid. Due to the interaction between the air/fluid and the solid, an elastic wave is excited inside the solid and the acoustic incident wave is scattered in the air/fluid. Such a scattering phenomenon leads to an acoustic-elastic interaction problem. The acoustic-elastic interaction problems have received great attention due to their significant applications in geophysics and seismology [32, 33]. These problems have been examined mathematically by using either variational method [4, 27] or boundary integral equation method [35, 46, 51]. Many computational approaches have also been developed to numerically solve these problems, such as boundary element method [25, 48] and coupling of finite and boundary element methods [24].

Since the acoustic-elastic interaction problem is imposed in an open domain, the unbounded physical domain needs to be truncated into a bounded computational domain to apply the numerical methods, such as the finite difference method, the finite element method and so on. Besides, an appropriate boundary condition is required on the boundary of the truncated domain to avoid artificial wave reflection. Such a boundary condition is called the transparent boundary condition (TBC) or non-reflecting boundary condition, which is an important and active subject in the research area of wave propagation [13, 22, 26, 28–30]. Since a perfectly matched layer (PML) technique was proposed by Berenger to solve the time-dependent Maxwell equations [14], the research on the PML has undergone a great development due to its effectiveness and simplicity. Various constructions of PML have been proposed for various scattering problems about the acoustic, elastic and electromagnetic wave propagation [10, 15, 17, 21, 31, 38–40]. The basic idea of the PML technique is to surround the domain of interest by a layer of finite thickness fictitious medium that attenuates the waves coming from inside of the computational domain. When the waves reach the outer boundary of the PML region, their values are so small that the homogeneous Dirichlet boundary conditions can be imposed.

The a posteriori error estimates are computable quantities measuring the errors between discrete problems and original problems, which are also essential to design the adaptive finite element algorithms. Based on the a posteriori error estimates, the adaptive finite element methods have the ability of error control and asymptotically optimal approximation property [3]. Because of these advantages, the adaptive finite element methods have become a class of effective numerical methods for solving differential equations, especially for those whose solutions have singularity or multiscale phenomena. Combined with the PML technique, an efficient adaptive finite element method was developed in [19] for solving the two-dimensional diffraction grating problems. It was shown that the a posteriori error estimate consists of the finite element discretization error and the PML truncation error, where the latter decays exponentially with respect to the PML parameters such as the thickness of the layer and the medium properties. Due to the superior numerical performance, the adaptive finite element PML method was quickly extended to solve many other scattering prob-

lems [7, 17, 18, 20, 39]. Based on the a posteriori error analysis, the adaptive finite element PML method provides an effective numerical strategy to solve various wave propagation problems imposed in unbounded domains.

As an alternative to the adaptive finite element PML method, the adaptive finite element DtN method (DtN-FEM) has also been proposed to solve the obstacle scattering problems [8, 11, 12, 36, 37, 45], the diffraction grating problems [5, 41, 43, 49, 53], and the open cavity scattering problem [52], where the transparent boundary conditions are used to truncate the unbounded domain. In this new approach, the layer of artificial medium is no longer needed to enclose the domain of interest, which is different from the PML method. Since the transparent boundary conditions are exact, the artificial boundary can be chosen to closely surround the domain of interest, which can significantly reduce the size of the computational domain. These transparent boundary conditions are based on nonlocal DtN operators and are given as infinite Fourier series. In practical computation, the infinite series needs to be truncated into a sum of finite number of terms by choosing an appropriate truncation parameter N. For theoretical analysis, the a posteriori error analysis technique of the adaptive finite element PML method cannot be applied directly to the adaptive finite element DtN method. To overcome such a difficulty, a new duality argument has been developed in [49] to obtain the a posteriori error estimate of the DtN-FEM. Comparably, the a posteriori error estimates consist of the finite element discretization error and the DtN truncation error, where the latter decays exponentially with respect to the truncation parameter N. The numerical experiments also demonstrate that the adaptive DtN-FEM method is as effective as the adaptive finite element PML method [37, 49].

In this paper, we present an adaptive DtN-FEM and carry out its mathematical analysis for the acoustic-elastic interaction problem. The contribution is twofold: (1) give a complete a posteriori error estimate; (2) develop an effective adaptive finite element algorithm. This paper extends the work from the acoustic obstacle scattering problem [37] to the acoustic-elastic interaction problem. It is worthy to mention that the extension is nontrivial. For such an acoustic-elastic interaction problem, we need to impose the kinematic and kinetic interface conditions on the fluid-solid interface to ensure the continuity of the velocity normal component and the traction, respectively. Due to the coupling of different physical fields and the complex transmission conditions, the original model problem and the associated variational problem of the acoustic-elastic interaction are much more complicated than those problems with single wave field. In the analysis of the a posteriori error, we need to estimate two line integral terms defined on the fluid-solid interface, which is different from the previous work about the single medium scattering. We give the corresponding error indicators of acoustic and elastic waves in different regions, which can reflect the distribution and magnitude of the errors of different physical fields in the computation.

The outline of this paper is as follows. In Sect. 2, we introduce the model of the acoustic-elastic interaction problem and its weak formulation by using the transparent boundary condition. The finite element discretization with truncated DtN operator is presented in Sect. 3, while the a posteriori error estimate is derived in Sect. 4 by using the duality argument method. In Sect. 5, we discuss the numerical implementation of our adaptive algorithm and present some numerical experiments to demonstrate the

effectiveness of the proposed method. Eventually, the paper is concluded with some general remarks and directions for future research in Sect. 6.

For brevity, we use the notation $a \lesssim b$ to imply that $a \leq Cb$, where the positive constant C is independent of the truncation parameter of the DtN operator and the mesh size of the triangulation.

2 Model problem

Let $\Omega_s \subset \mathbb{R}^2$ be a bounded domain with a Lipschitz boundary Γ, and $\Omega_e = \mathbb{R}^2 \backslash \overline{\Omega}_s$ be the unbounded connected exterior region. The domain Ω_s is occupied by a linear and isotropic elastic solid determined through the Lamé constants μ and λ ($\mu > 0$ and $\lambda + \mu > 0$) , and its mass density $\rho > 0$. The domain Ω_e is filled with a homogeneous, compressible, and inviscid air/fluid with a constant density $\rho_f > 0$. Let $B_R = \{\boldsymbol{x} \in \mathbb{R}^2 : |\boldsymbol{x}| < R\}$ and $B_{R'} = \{\boldsymbol{x} \in \mathbb{R}^2 : |\boldsymbol{x}| < R'\}$ be the balls with radius R and R', respectively, where $R > R' > 0$. Assume that R' is large enough such that $\overline{\Omega}_s \subset B_{R'} \subset B_R$. The model geometry of the acoustic-elastic interaction is shown in Fig. 1. Denote by $\boldsymbol{n} = (n_1, n_2)^\top$ the unit normal vector to Γ dircted into Ω_e.

Let the elastic solid be impinged by a time-harmonic sound wave p^i, which satisfies the two-dimensional Helmholtz equation

$$\triangle p^i + \kappa^2 p^i = 0 \quad \text{in } \Omega_e,$$

where $\kappa = \omega/c$ is the wavenumber, $\omega > 0$ is the angular frequency, and c is the speed of sound in the air/fluid. The total acoustic wave field p^t also satisfies the Helmholtz

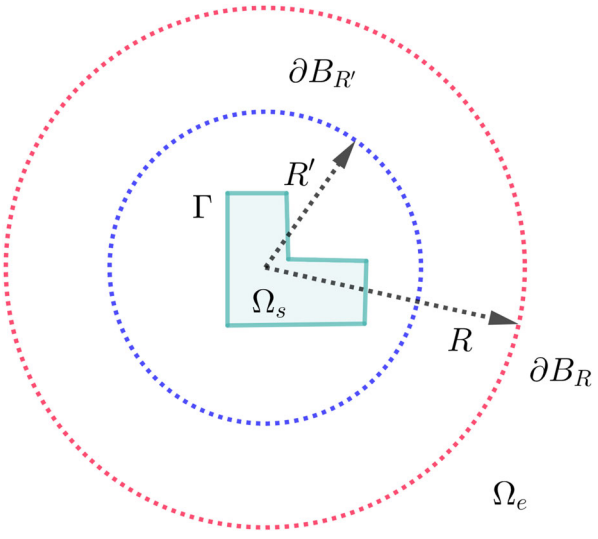

Fig. 1 A two-dimensional schematic of the problem geometry for the acoustic-elastic interaction

equation

$$\triangle p^t + \kappa^2 p^t = 0 \quad \text{in } \Omega_e.$$

The total field p^t consists of the incident field p^i and the scattered field p^s, i.e.,

$$p^t = p^i + p^s \quad \text{in } \Omega_e,$$

where p^s is required to satisfy the Sommerfeld radiation condition

$$\lim_{r\to\infty} \sqrt{r}\left(\partial_r p^s - i\kappa p^s\right) = 0, \quad r = |\boldsymbol{x}|.$$

When the acoustic wave hits the surface of the penetrable elastic obstacle, it excites an elastic wave inside the obstacle. The elastic wave satisfies the two-dimensional Navier equation

$$\triangle^* \boldsymbol{u} + \rho\omega^2 \boldsymbol{u} = 0 \quad \text{in } \Omega_s,$$

where $\triangle^* := \mu\triangle + (\lambda+\mu)\nabla\nabla\cdot$, and $\boldsymbol{u} = (u_1, u_2)^\top$ is the displacement of the elastic wave. To ensure the continuity of the normal component of the velocity, the kinematic interface condition is imposed on the fluid-solid interface

$$\partial_{\boldsymbol{n}} p^t = \rho_f \omega^2 \boldsymbol{u}\cdot\boldsymbol{n} \quad \text{on } \Gamma. \tag{1}$$

Additionally, the following dynamic interface condition is also required to ensure the continuity of traction

$$-p^t \boldsymbol{n} = \boldsymbol{T}\boldsymbol{u} \quad \text{on } \Gamma, \tag{2}$$

where the traction operator $\boldsymbol{T}$ is defined as

$$\boldsymbol{T}\boldsymbol{u} := 2\mu\partial_{\boldsymbol{n}}\boldsymbol{u} + \lambda\boldsymbol{n}\nabla\cdot\boldsymbol{u} + \mu\begin{pmatrix} n_2\left(\frac{\partial u_2}{\partial x} - \frac{\partial u_1}{\partial y}\right) \\ n_1\left(\frac{\partial u_1}{\partial y} - \frac{\partial u_2}{\partial x}\right)\end{pmatrix}.$$

Thus, the acoustic-elastic interaction problem can be formulated as: Given p^i, to find $p^s \in C^2(\Omega_e)\cap C^1\left(\overline{\Omega}_e\right)$ and $\boldsymbol{u} \in \left(C^2(\Omega_s)\cap C^1(\overline{\Omega}_s)\right)^2$ such that

$$\begin{aligned} \triangle p^s + \kappa^2 p^s &= 0 \quad \text{in } \Omega_e, \\ \triangle^* \boldsymbol{u} + \rho\omega^2\boldsymbol{u} &= 0 \quad \text{in } \Omega_s, \\ \partial_{\boldsymbol{n}} p^t &= \rho_f\omega^2\boldsymbol{u}\cdot\boldsymbol{n} \quad \text{on } \Gamma, \\ -p^t\boldsymbol{n} &= \boldsymbol{T}\boldsymbol{u} \quad \text{on } \Gamma, \\ \left(\partial_r p^s - \mathrm{i}\kappa p^s\right) &= o(r^{1/2}) \quad \text{as } r\to\infty. \end{aligned} \tag{3}$$

It follows from [42] that the problem (3) is not always uniquely solvable due to the occurrence of traction free oscillations for certain geometries and some frequencies ω. These special ω are also named by the Jones frequencies, which are inherent to the original model. One can obtain the following uniqueness result of the problem (3); see also [46].

Lemma 1 *If the surface* Γ *and the material parameters* (μ, λ, ρ) *are such that there are no traction free solutions, the boundary value problem* (3) *has at most one solution. Here, the nontrivial* $\boldsymbol{u_0}$ *is a traction free solution if it satisfies*

$$\begin{aligned} \triangle^* \boldsymbol{u}_0 + \rho\omega^2 \boldsymbol{u}_0 &= 0 \quad \text{in } \Omega_s, \\ \boldsymbol{T}\boldsymbol{u}_0 &= 0 \quad \text{on } \Gamma, \\ \boldsymbol{u}_0 \cdot \boldsymbol{n} &= 0 \quad \text{on } \Gamma. \end{aligned}$$

Since the problem (3) is imposed in an unbounded domain, we introduce the transparent boundary condition to truncate the unbounded domain. For any $p \in L^2(\partial B_R)$, it admits the Fourier series expansion

$$p(R,\theta) = \sum_{n\in\mathbb{Z}} \hat{p}_n(R) e^{\mathrm{i}n\theta}, \quad \hat{p}_n(R) = \frac{1}{2\pi}\int_0^{2\pi} p(R,\theta) e^{-\mathrm{i}n\theta}\mathrm{d}\theta.$$

The equivalent $L^2(\partial B_R)$ norm of p is defined as

$$\|p\|_{L^2(\partial B_R)} = \left(2\pi \sum_{n\in\mathbb{Z}} |\hat{p}_n(R)|^2\right)^{1/2}.$$

The trace space $H^s(\partial B_R)$ is defined by

$$H^s(\partial B_R) = \{p \in L^2(\partial B_R) : \|p\|_{H^s(\partial B_R)} < \infty\},$$

where the $H^s(\partial B_R)$ norm is given as

$$\|p\|_{H^s(\partial B_R)} = \left(2\pi \sum_{n\in\mathbb{Z}} (1+n^2)^s |\hat{p}_n(R)|^2\right)^{1/2}.$$

The dual space of $H^s(\partial B_R)$ is $H^{-s}(\partial B_R)$ with respect to the scalar product in $L^2(\partial B_R)$ defined by

$$\langle p, q\rangle_{\partial B_R} = \int_{\partial B_R} p\overline{q}\mathrm{d}s.$$

In the exterior domain $\mathbb{R}^2\backslash\overline{B}_R$, the solution of the Helmholtz equation can be written as an infinite Fourier series in the polar coordinates, i.e.,

$$p(r,\theta) = \sum_{n\in\mathbb{Z}} \frac{H_n^{(1)}(\kappa r)}{H_n^{(1)}(\kappa R)} \hat{p}_n(R) e^{\mathrm{i}n\theta}, \quad r \geq R, \tag{4}$$

$$\hat{p}_n(R) = \frac{1}{2\pi}\int_0^{2\pi} p(R,\theta) e^{-\mathrm{i}n\theta}\mathrm{d}\theta,$$

where $H_n^{(1)}(\cdot)$ is the Hankel function of the first kind with order n. Given $p \in H^{1/2}(\partial B_R)$, introduce the DtN operator $\mathscr{T} : H^{1/2}(\partial B_R) \to H^{-1/2}(\partial B_R)$, defined by

$$\mathscr{T} p(R,\theta) = \frac{1}{R} \sum_{n\in\mathbb{Z}} h_n(\kappa R)\hat{p}_n(R) e^{\mathrm{i}n\theta}, \tag{5}$$

where

$$h_n(z) = z \frac{H_n^{(1)'}(z)}{H_n^{(1)}(z)}.$$

It follows from (4) and (5) that the transparent boundary condition can be defined as

$$\partial_r p = \mathscr{T} p \quad \text{on } \partial B_R.$$

Denote truncated region by Ω_a. Assume that $\Omega = \Omega_a \cup \Omega_s$. By the DtN operator $\mathscr{T}$, we can reformulate the boundary value problem (3) from the unbounded domain into the bounded domain as: Given p^i, to find p^s and $\boldsymbol{u}$ such that

$$\begin{aligned} \triangle p^s + \kappa^2 p^s &= 0 \quad \text{in } \Omega_a, \\ \triangle^* \boldsymbol{u} + \rho\omega^2 \boldsymbol{u} &= 0 \quad \text{in } \Omega_s, \\ \partial_{\boldsymbol{n}} p^t &= \rho_f \omega^2 \boldsymbol{u}\cdot\boldsymbol{n} \quad \text{on } \Gamma, \\ -p^t \boldsymbol{n} &= \boldsymbol{T}\boldsymbol{u} \quad \text{on } \Gamma, \\ \partial_r p^s &= \mathscr{T} p^s \quad \text{on } \partial B_R. \end{aligned} \tag{6}$$

The uniqueness result of the nonlocal boundary value problem (6) is introduced in Lemma 2.

Lemma 2 (See [50]) *If the surface* Γ *and the material parameter* (μ, λ, ρ) *are such that there are no traction free solutions, the nonlocal boundary value problem* (6) *has at most one solution.*

To carry out the theoretical analysis, we introduce the space

$$\mathcal{H}^1(\Omega) := H^1(\Omega_a) \times H^1(\Omega_s)^2 = \{U = (p, \boldsymbol{u}) : p \in H^1(\Omega_a), \boldsymbol{u} \in H^1(\Omega_s)^2\},$$

which is endowed with the inner product

$$\begin{aligned} (\boldsymbol{U}, \boldsymbol{V})_{\mathcal{H}} := &\int_{\Omega_s} \left(\lambda(\nabla\cdot\boldsymbol{u})(\nabla\cdot\overline{\boldsymbol{v}}) + \frac{\mu}{2}(\nabla\boldsymbol{u} + \nabla\boldsymbol{u}^\top) : (\nabla\overline{\boldsymbol{v}} + \nabla\overline{\boldsymbol{v}}^\top) + \boldsymbol{u}\cdot\overline{\boldsymbol{v}}\right) \mathrm{d}\boldsymbol{x} \\ &+ \int_{\Omega_a} (\nabla p \cdot \nabla\overline{q} + p\overline{q})\, \mathrm{d}\boldsymbol{x} \end{aligned}$$

for any $\boldsymbol{U} = (p, \boldsymbol{u})$ and $\boldsymbol{V} = (q, \boldsymbol{v})$. Here, $A : B = \mathrm{tr}(AB^\top)$ is the Frobenius inner product of square matrices A and B, and $\nabla\boldsymbol{u}$ is the displacement gradient tensor, which

is given by

$$\nabla \boldsymbol{u} = \begin{bmatrix} \frac{\partial u_1}{\partial x} & \frac{\partial u_1}{\partial y} \\ \frac{\partial u_2}{\partial x} & \frac{\partial u_2}{\partial y} \end{bmatrix}.$$

Obviously, $\|\cdot\|_{\mathcal{H}^1(\Omega)} = \sqrt{(\cdot,\cdot)_{\mathcal{H}}}$ is a norm on $\mathcal{H}^1(\Omega)$. For convenience, we introduce the first generalized Betti formula; see also [1].

Lemma 3 *Let $D \subset \mathbb{R}^2$ be a domain in which the divergence theorem holds. Then, for any vector fields $\boldsymbol{u} \in C^2(\overline{D})^2$ and $\boldsymbol{v} \in C^1(\overline{D})^2$, the first generalized Betti formula holds:*

$$\int_D \triangle^* \boldsymbol{u} \cdot \boldsymbol{v} \mathrm{d}\boldsymbol{x} + \int_D \mathcal{E}_{\lambda,\mu}(\boldsymbol{u}, \boldsymbol{v}) \mathrm{d}\boldsymbol{x} = \int_{\partial D} \boldsymbol{T}\boldsymbol{u} \cdot \boldsymbol{v} \mathrm{d}s,$$

where

$$\begin{aligned} \mathcal{E}_{\lambda,\mu}(\boldsymbol{u}, \boldsymbol{v}) &= (2\mu + \lambda)\left(\frac{\partial u_1}{\partial x}\frac{\partial v_1}{\partial x} + \frac{\partial u_2}{\partial y}\frac{\partial v_2}{\partial y}\right) + \mu\left(\frac{\partial u_1}{\partial y}\frac{\partial v_1}{\partial y} + \frac{\partial u_2}{\partial x}\frac{\partial v_2}{\partial x}\right) \\ &\quad + \lambda\left(\frac{\partial u_2}{\partial y}\frac{\partial v_1}{\partial x} + \frac{\partial u_1}{\partial x}\frac{\partial v_2}{\partial y}\right) + \mu\left(\frac{\partial u_2}{\partial x}\frac{\partial v_1}{\partial y} + \frac{\partial u_1}{\partial y}\frac{\partial v_2}{\partial x}\right) \\ &= \lambda(\nabla \cdot \boldsymbol{u})(\nabla \cdot \boldsymbol{v}) + \frac{\mu}{2}(\nabla \boldsymbol{u} + \nabla \boldsymbol{u}^\top) : (\nabla \boldsymbol{v} + \nabla \boldsymbol{v}^\top). \end{aligned}$$

It follows from (6), Green's formula and Lemma 3 that

$$\begin{aligned} 0 &= \int_{\Omega_a} \left(\triangle p^s \overline{q} + \kappa^2 p^s \overline{q}\right) \mathrm{d}\boldsymbol{x} \\ &= \int_{\Omega_a} \left(-\nabla p^s \cdot \nabla \overline{q} + \kappa^2 p^s \overline{q}\right) \mathrm{d}\boldsymbol{x} - \int_\Gamma \rho_f \omega^2 \boldsymbol{u} \cdot \boldsymbol{n} \overline{q} \mathrm{d}s + \int_{\partial B_R} \mathscr{T} p^s \overline{q} \mathrm{d}s + \int_\Gamma \partial_{\boldsymbol{n}} p^i \overline{q} \mathrm{d}s \end{aligned}$$

and

$$\begin{aligned} 0 &= \int_{\Omega_s} \left(\triangle^* \boldsymbol{u} \cdot \boldsymbol{v} + \rho\omega^2 \boldsymbol{u} \cdot \overline{\boldsymbol{v}}\right) \mathrm{d}\boldsymbol{x} \\ &= \int_{\Omega_s} \left(-\mathcal{E}_{\lambda,\mu}(\boldsymbol{u}, \boldsymbol{v}) + \rho\omega^2 \boldsymbol{u} \cdot \overline{\boldsymbol{v}}\right) \mathrm{d}\boldsymbol{x} + \int_{\partial\Omega_s} \boldsymbol{T}\boldsymbol{u} \cdot \overline{\boldsymbol{v}} \mathrm{d}s \\ &= \int_{\Omega_s} \left(-\mathcal{E}_{\lambda,\mu}(\boldsymbol{u}, \boldsymbol{v}) + \rho\omega^2 \boldsymbol{u} \cdot \overline{\boldsymbol{v}}\right) \mathrm{d}\boldsymbol{x} - \int_\Gamma p^s \boldsymbol{n} \cdot \overline{\boldsymbol{v}} \mathrm{d}s - \int_\Gamma p^i \boldsymbol{n} \cdot \overline{\boldsymbol{v}} \mathrm{d}s. \end{aligned}$$

Let $A : \mathcal{H}^1(\Omega) \times \mathcal{H}^1(\Omega) \to \mathbb{C}$ be the sesquilinear form defined by

$$A(\boldsymbol{U}, \boldsymbol{V}) = a_1(\boldsymbol{u}, \boldsymbol{v}) + a_2(p^s, q) + a_3(\boldsymbol{u}, q) + a_4(p^s, \boldsymbol{v}) + b(p^s, q), \tag{7}$$

where

$$
\begin{aligned}
a_1(\boldsymbol{u}, \boldsymbol{v}) &= \int_{\Omega_s} \left(\mathcal{E}_{\lambda,\mu}(\boldsymbol{u}, \boldsymbol{v}) - \rho\omega^2 \boldsymbol{u} \cdot \overline{\boldsymbol{v}} \right) \mathrm{d}\boldsymbol{x}, \\
a_2(p^s, q) &= \int_{\Omega_a} \left(\nabla p^s \cdot \nabla \overline{q} - \kappa^2 p^s \overline{q} \right) \mathrm{d}\boldsymbol{x}, \\
a_3(\boldsymbol{u}, q) &= \int_{\Gamma} \rho_f \omega^2 \boldsymbol{u} \cdot \boldsymbol{n} \overline{q} \mathrm{d}s, \\
a_4(p^s, \boldsymbol{v}) &= \int_{\Gamma} p^s \boldsymbol{n} \cdot \overline{\boldsymbol{v}} \mathrm{d}s, \\
b(p^s, q) &= -\int_{\partial B_R} \mathscr{T} p^s \overline{q} \mathrm{d}s,
\end{aligned}
$$

and ℓ be the bounded linear functional as

$$
\ell(\boldsymbol{V}) = \int_{\Gamma} \partial_{\boldsymbol{n}} p^i \overline{q} - p^i \boldsymbol{n} \cdot \overline{\boldsymbol{v}} \mathrm{d}s. \tag{8}
$$

Thus, we arrive at an equivalent variational formulation of the acoustic-elastic interaction problem (6): Given p^i, to find $\boldsymbol{U} = (p^s, \boldsymbol{u}) \in \mathcal{H}^1(\Omega)$ such that

$$
A(\boldsymbol{U}, \boldsymbol{V}) = \ell(\boldsymbol{V}) \quad \text{for all } \boldsymbol{V} = (q, \boldsymbol{v}) \in \mathcal{H}^1(\Omega). \tag{9}
$$

It follows from [50] that we have the following uniqueness result of the variational problem (9).

Lemma 4 *Let the surface Γ and the material parameter (μ, λ, ρ) be such that there are no traction free solutions, then the variational equation (9) admits a unique solution.*

The general theory in Babuška and Aziz [2] implies that there exists a constant β such that the following inf-sup condition holds

$$
\sup_{0 \neq \boldsymbol{V} \in \mathcal{H}^1(\Omega)} \frac{|A(\boldsymbol{U}, \boldsymbol{V})|}{\|\boldsymbol{V}\|_{\mathcal{H}^1(\Omega)}} \geq \beta \|\boldsymbol{U}\|_{\mathcal{H}^1(\Omega)} \quad \text{for all } \boldsymbol{U} \in \mathcal{H}^1(\Omega). \tag{10}
$$

It follows from (8), (9) and (10) that

$$
\|\boldsymbol{U}\|_{\mathcal{H}^1(\Omega)} \lesssim \left\| p^i \right\|_{H^1(\Gamma)} \lesssim \left\| p^i \right\|_{H^2(\Omega_a)}. \tag{11}
$$

3 Finite element approximation

Denote by $\mathcal{M}_{h,s}$ and $\mathcal{M}_{h,a}$ the regular triangulations of Ω_s and Ω_a, respectively. Let $\mathcal{M}_h = \mathcal{M}_{h,s} \cup \mathcal{M}_{h,a}$. To avoid being distracted from the main focus of the a posteriori error estimate, we assume for simplicity that Γ and ∂B_R are polygonals to keep from

using the isoparametric finite element space and deriving the approximation error of Γ and ∂B_R.

Let $\hat{S}_h \subset H^1(\Omega_a)$ and $\overline{S}_h \subset H^1(\Omega_s)^2$ be the conforming finite element spaces, i.e.,

$$\hat{S}_h := \{p_h \in C(\overline{\Omega}_a) : p_h|_K \in P_m(K) \text{ for all } K \in \mathcal{M}_{h,a}\},$$
$$\overline{S}_h := \{\boldsymbol{u}_h \in C(\overline{\Omega}_s) : \boldsymbol{u}_h|_K \in P_m(K)^2 \text{ for all } K \in \mathcal{M}_{h,s}\},$$

where m is a positive integer and $P_m(K)$ denotes the set of all polynomials of degree no more than m. Let $\mathcal{H}_h^1(\Omega) := \hat{S}_h \times \overline{S}_h \subset \mathcal{H}^1(\Omega)$. The finite element approximation to the problem (9) reads as follows: Given p^i, to find $\boldsymbol{U}_h = (p_h^s, \boldsymbol{u}_h) \in \mathcal{H}_h^1(\Omega)$ such that

$$A(\boldsymbol{U}_h, \boldsymbol{V}_h) = \ell(\boldsymbol{V}_h) \quad \text{for all } \boldsymbol{V}_h = (q_h, \boldsymbol{v}_h) \in \mathcal{H}_h^1(\Omega), \tag{12}$$

where

$$\begin{aligned}
A(\boldsymbol{U}_h, \boldsymbol{V}_h) &= a_1(\boldsymbol{u}_h, \boldsymbol{v}_h) + a_2(p_h^s, q_h) + a_3(\boldsymbol{u}_h, q_h) + a_4(p_h^s, \boldsymbol{v}_h) + b(p_h^s, q_h),\\
a_1(\boldsymbol{u}_h, \boldsymbol{v}_h) &= \int_{\Omega_s} \left(\mathcal{E}_{\lambda,\mu}(\boldsymbol{u}_h, \boldsymbol{v}_h) - \rho\omega^2 \boldsymbol{u}_h \cdot \overline{\boldsymbol{v}}_h\right) \mathrm{d}\boldsymbol{x},\\
a_2(p_h^s, q_h) &= \int_{\Omega_a} \left(\nabla p_h^s \cdot \nabla \overline{q}_h - \kappa^2 p_h^s \overline{q}_h\right) \mathrm{d}\boldsymbol{x},\\
a_3(\boldsymbol{u}_h, q_h) &= \int_{\Gamma} \rho_f \omega^2 \boldsymbol{u}_h \cdot \boldsymbol{n} \overline{q}_h \mathrm{d}s,\\
a_4(p_h^s, \boldsymbol{v}_h) &= \int_{\Gamma} p_h^s \boldsymbol{n} \cdot \overline{\boldsymbol{v}}_h \mathrm{d}s,\\
b(p_h^s, q_h) &= -\int_{\partial B_R} \mathscr{T} p_h^s \overline{q}_h \mathrm{d}s,\\
\ell(\boldsymbol{V}_h) &= \int_{\Gamma} \partial_{\boldsymbol{n}} p^i \overline{q}_h - p^i \boldsymbol{n} \cdot \overline{\boldsymbol{v}}_h \mathrm{d}s.
\end{aligned}$$

In the above equations, the DtN operator $\mathscr{T}$ defined in (5) is given by an infinite series. In fact, it is necessary to truncate the nonlocal operator $\mathscr{T}$ by taking finitely many terms of the expansions so as to attain a feasible algorithm. Given a sufficiently large N, define the truncated DtN operator $\mathscr{T}_N$ as

$$(\mathscr{T}_N p)(R, \theta) = \frac{1}{R} \sum_{|n| \le N} h_n(\kappa R) \hat{p}_n(R) e^{\mathrm{i}n\theta}. \tag{13}$$

Using the truncated DtN operator, we obtain the truncated finite element approximation to the problem (9): Given p^i, to find $\boldsymbol{U}_h^N = (p_h^{s,N}, \boldsymbol{u}_h^N) \in \mathcal{H}_h^1(\Omega)$ such that

$$A^N(\boldsymbol{U}_h^N, \boldsymbol{V}_h) = \ell(\boldsymbol{V}_h) \quad \text{for all } \boldsymbol{V}_h \in \mathcal{H}_h^1(\Omega), \tag{14}$$

where

$$
\begin{aligned}
A^N\left(\boldsymbol{U}_h^N, \boldsymbol{V}_h\right) &= a_1(\boldsymbol{u}_h^N, \boldsymbol{v}_h) + a_2(p_h^{s,N}, q_h) + a_3(\boldsymbol{u}_h^N, q_h) + a_4(p_h^{s,N}, \boldsymbol{v}_h) + b^N(p_h^{s,N}, q_h),\\
a_1(\boldsymbol{u}_h^N, \boldsymbol{v}_h) &= \int_{\Omega_s} \left(\mathcal{E}_{\lambda,\mu}(\boldsymbol{u}_h^N, \boldsymbol{v}_h) - \rho\omega^2 \boldsymbol{u}_h^N \cdot \overline{\boldsymbol{v}}_h\right) \mathrm{d}\boldsymbol{x},\\
a_2(p_h^{s,N}, q_h) &= \int_{\Omega_a} \left(\nabla p_h^{s,N} \cdot \nabla \overline{q}_h - \kappa^2 p_h^{s,N} \overline{q}_h\right) \mathrm{d}\boldsymbol{x},\\
a_3(\boldsymbol{u}_h^N, q_h) &= \int_{\Gamma} \rho_f \omega^2 \boldsymbol{u}_h^N \cdot \boldsymbol{n} \overline{q}_h \mathrm{d}s,\\
a_4(p_h^{s,N}, \boldsymbol{v}_h) &= \int_{\Gamma} p_h^{s,N} \boldsymbol{n} \cdot \overline{\boldsymbol{v}}_h \mathrm{d}s,\\
b^N(p_h^{s,N}, q_h) &= -\int_{\partial B_R} \mathscr{T}_N p_h^{s,N} \overline{q}_h \mathrm{d}s.
\end{aligned}
$$

For sufficiently large N and sufficiently small h, we present the following result of uniqueness and existence of solutions to the truncted problem (14); see also [50].

Lemma 5 *Let the surface Γ and the material parameter (μ, λ, ρ) be such that there are no traction free solutions, then there exists a constant $N_0 \geq 0$ such that the truncted equation (14) admits a unique solution $\boldsymbol{U}_h^N = (p_h^{s,N}, \boldsymbol{u}_h^N) \in \mathcal{H}_h^1(\Omega)$ for $N \geq N_0$.*

We also refer to [50] for error analysis of the problem (14). In this work, we mainly focus on the a posteriori error estimate and the associated adaptive algorithm.

4 The a posteriori error analysis

For any $K \in \mathcal{M}_h$, denote by h_K its diameter. Let $\mathcal{B}_h$ denote the set of all edges of K. For any $e \in \mathcal{B}_h$, denote by h_e its length. For $K \in \mathcal{M}_{h,a}$ and $K \in \mathcal{M}_{h,s}$, denote the jump residual across the edge of K as $J_{e,a}$ and $\boldsymbol{J_{e,s}}$, respectively.

For any interior edge e which is the common side of $K_1, K_2 \in \mathcal{M}_{h,a}$, define the jump residual across e as

$$
J_{e,a} = -\left(\nabla p_h^{s,N}|_{K_1} \cdot \boldsymbol{\nu}_1 + \nabla p_h^{s,N}|_{K_2} \cdot \boldsymbol{\nu}_2\right),
$$

where $\boldsymbol{\nu}_j$ is the unit outward normal vector to the boundary of K_j, $j = 1, 2$. For any boundary edge $e \in \partial B_R$, define the jump residual

$$
J_{e,a} = 2\left(\mathscr{T}_N p_h^{s,N} - \nabla p_h^{s,N} \cdot \boldsymbol{\nu}\right),
$$

where $\boldsymbol{\nu}$ is the unit outward normal to ∂B_R. For any boundary edge $e \in \Gamma$, define the jump residual

$$
\begin{aligned}
J_{e,a} &= 2\left(\partial_{\boldsymbol{n}}(p^i + p_h^{s,N}) - \rho_f \omega^2 \boldsymbol{u}_h^N \cdot \boldsymbol{n}\right),\\
\boldsymbol{J_{e,s}} &= -2\left((p^i + p_h^{s,N})\boldsymbol{n} + \boldsymbol{T}\boldsymbol{u}_h^N\right).
\end{aligned}
$$

For any interior edge e which is the common side of $K_1, K_2 \in \mathcal{M}_{h,s}$, define the jump residual across e as

$$\boldsymbol{J_{e,s}} = -\left(\boldsymbol{T}\boldsymbol{u}_h^N|_{K_1} + \boldsymbol{T}\boldsymbol{u}_h^N|_{K_2}\right).$$

For $K \in \mathcal{M}_{h,a}$ and $K \in \mathcal{M}_{h,s}$, denote the local error estimators by $\eta_{K,a}$ and $\eta_{K,s}$, which is defined respectively by

$$\eta_{K,a} = h_K \left\| \mathcal{R}_a p_h^{s,N} \right\|_{L^2(K)} + \left(\frac{1}{2} \sum_{e \in \partial_K} h_e \| J_{e,a} \|_{L^2(e)}^2 \right)^{1/2}, \tag{15}$$

$$\eta_{K,s} = h_K \left\| \mathcal{R}_s \boldsymbol{u}_h^N \right\|_{L^2(K)} + \left(\frac{1}{2} \sum_{e \in \partial_K} h_e \| \boldsymbol{J_{e,s}} \|_{L^2(e)}^2 \right)^{1/2}, \tag{16}$$

where the residual operator $\mathcal{R}_a := \triangle + \kappa^2$ and $\mathcal{R}_s := \triangle^* + \rho\omega^2$.

Denote the error by $\boldsymbol{\Psi} = (\xi, \boldsymbol{\zeta}) \in \mathcal{H}^1(\Omega)$, where $\xi := p^s - p_h^{s,N}$, $\boldsymbol{\zeta} := \boldsymbol{u} - \boldsymbol{u}_h^N$. Introduce a dual problem to the original scattering problem: Find $\boldsymbol{\Phi} = (\gamma, \boldsymbol{w}) \in \mathcal{H}^1(\Omega)$ such that

$$A(\boldsymbol{V}, \boldsymbol{\Phi}) = (\boldsymbol{V}, \boldsymbol{\Psi}) \quad \text{for all } \boldsymbol{V} = (q, \boldsymbol{v}) \in \mathcal{H}^1(\Omega), \tag{17}$$

where

$$A(\boldsymbol{V}, \boldsymbol{\Phi}) = A(q, \boldsymbol{v}; \gamma, \boldsymbol{w}),$$

and

$$(\boldsymbol{V}, \boldsymbol{\Psi}) = (q, \boldsymbol{v}; \xi, \boldsymbol{\zeta}).$$

It can be verified that $\boldsymbol{\Phi}$ is the weak solution to the following boundary value problem

$$\begin{aligned}
\triangle\gamma + \kappa^2\gamma &= -\xi \quad \text{in } \Omega_a, \\
\triangle^*\boldsymbol{w} + \rho\omega^2\boldsymbol{w} &= -\boldsymbol{\zeta} \quad \text{in } \Omega_s, \\
\partial_{\boldsymbol{n}}\gamma &= \boldsymbol{w} \cdot \boldsymbol{n} \quad \text{on } \Gamma, \\
-\rho_f\omega^2\gamma\boldsymbol{n} &= T\boldsymbol{w} \quad \text{on } \Gamma, \\
\partial_r\gamma &= \mathscr{T}^*\gamma \quad \text{on } \partial B_R,
\end{aligned}$$

where the adjoint operator $\mathscr{T}^*$ is defined as

$$(\mathscr{T}^*\gamma)(R, \theta) = \frac{1}{R} \sum_{n \in \mathbb{Z}} \overline{h}_n(\kappa R)\hat{\gamma}_n(R) e^{in\theta}.$$

Following the same proof as that for the original scattering problem (9), we may show that the dual problem (17) has a unique weak solution, which satisfies the estimate

$$\|\mathbf{\Phi}\|_{\mathcal{H}^1(\Omega)} \lesssim \|\mathbf{\Psi}\|_{L^2(\Omega)}. \tag{18}$$

The following lemma gives some energy representations of the error $\mathbf{\Psi}$ and is the basis for the a posteriori error analysis.

Lemma 6 *Let* $(p^s, \boldsymbol{u})$, $(p_h^{s,N}, \boldsymbol{u}_h^N)$ *and* $\mathbf{\Phi} = (\gamma, \boldsymbol{w})$ *be the solutions to the problems* (9), (14) *and* (17), *respectively. We have*

$$\|\mathbf{\Psi}\|^2_{L^2(\Omega)} = A(\mathbf{\Psi}, \mathbf{\Phi}) + \langle(\mathscr{T} - \mathscr{T}_N)\xi, \gamma\rangle_{\partial B_R} - \langle(\mathscr{T} - \mathscr{T}_N)\xi, \gamma\rangle_{\partial B_R}, \tag{19}$$

$$\begin{aligned}\|\mathbf{\Psi}\|^2_{\mathcal{H}^1(\Omega)} =& \mathrm{Re}\left(A(\mathbf{\Psi}, \mathbf{\Psi}) + \langle(\mathscr{T} - \mathscr{T}_N)\xi, \xi\rangle_{\partial B_R}\right) + \mathrm{Re}\langle\mathscr{T}_N\xi, \xi\rangle_{\partial B_R} \\ &+ (\rho\omega^2 + 1)\|\boldsymbol{\zeta}\|^2_{L^2(\Omega_s)} + (\kappa^2 + 1)\|\xi\|^2_{L^2(\Omega_a)} - \mathrm{Re}\left(a_3(\boldsymbol{\zeta}, \xi) + a_4(\xi, \boldsymbol{\zeta})\right),\end{aligned} \tag{20}$$

$$\begin{aligned}A(\mathbf{\Psi}, \boldsymbol{V}) + \langle(\mathscr{T} - \mathscr{T}_N)\xi, q\rangle_{\partial B_R} =& \ell(q - q_h, \boldsymbol{v} - \boldsymbol{v}_h) - A^N\left(p_h^{s,N}, \boldsymbol{u}_h^N; q - q_h, \boldsymbol{v} - \boldsymbol{v}_h\right) \\ &+ \langle(\mathscr{T} - \mathscr{T}_N)p^s, q\rangle_{\partial B_R}, \quad \forall\, \boldsymbol{V} \in \mathcal{H}^1(\Omega), \boldsymbol{V}_h \in \mathcal{H}_h^1(\Omega).\end{aligned} \tag{21}$$

Proof Taking $\boldsymbol{V} = \mathbf{\Psi}$ in (17) gives (19). It follows from the definition of the sesquilinear form of A in (7) that

$$A(\mathbf{\Psi}, \mathbf{\Psi}) = a_1(\boldsymbol{\zeta}, \boldsymbol{\zeta}) + a_2(\xi, \xi) + a_3(\boldsymbol{\zeta}, \xi) + a_4(\xi, \boldsymbol{\zeta}) + b(\xi, \xi),$$

which gives

$$\|\mathbf{\Psi}\|^2_{\mathcal{H}^1(\Omega)} = A(\mathbf{\Psi}, \mathbf{\Psi}) + \langle\mathscr{T}\xi, \xi\rangle_{\partial B_R} + (\rho\omega^2 + 1)\|\boldsymbol{\zeta}\|^2_{L^2(\Omega_s)} + (\kappa^2 + 1)\|\xi\|^2_{L^2(\Omega_a)} - a_3(\boldsymbol{\zeta}, \xi) - a_4(\xi, \boldsymbol{\zeta}).$$

Taking the real parts on both sides of the above equation yields (20). It remains to prove (21).

It follows from (9) and (14) that

$$\begin{aligned}A(\mathbf{\Psi}, \boldsymbol{V}) &= A\left(p^s - p_h^{s,N}, \boldsymbol{u} - \boldsymbol{u}_h^N; q - q_h, \boldsymbol{v} - \boldsymbol{v}_h\right) + A\left(p^s - p_h^{s,N}, \boldsymbol{u} - \boldsymbol{u}_h^N; q_h, \boldsymbol{v}_h\right) \\ &= A\left(p^s, \boldsymbol{u}; q - q_h, \boldsymbol{v} - \boldsymbol{v}_h\right) - A\left(p_h^{s,N}, \boldsymbol{u}_h^N; q - q_h, \boldsymbol{v} - \boldsymbol{v}_h\right) \\ &\quad + A\left(p^s - p_h^{s,N}, \boldsymbol{u} - \boldsymbol{u}_h^N; q_h, \boldsymbol{v}_h\right) \\ &= \ell(q - q_h, \boldsymbol{v} - \boldsymbol{v}_h) - A^N\left(p_h^{s,N}, \boldsymbol{u}_h^N; q - q_h, \boldsymbol{v} - \boldsymbol{v}_h\right) \\ &\quad + A^N\left(p_h^{s,N}, \boldsymbol{u}_h^N; q - q_h, \boldsymbol{v} - \boldsymbol{v}_h\right) - A\left(p_h^{s,N}, \boldsymbol{u}_h^N; q - q_h, \boldsymbol{v} - \boldsymbol{v}_h\right) \\ &\quad + A\left(p^s, \boldsymbol{u}; q_h, \boldsymbol{v}_h\right) - A\left(p_h^{s,N}, \boldsymbol{u}_h^N; q_h, \boldsymbol{v}_h\right).\end{aligned}$$

Noting that $A\left(p^s, \boldsymbol{u}; q_h, \boldsymbol{v}_h\right) = \ell(q_h, \boldsymbol{v}_h) = A^N\left(p_h^{s,N}, \boldsymbol{u}_h^N; q_h, \boldsymbol{v}_h\right)$, we have

$$\begin{aligned} A(\boldsymbol{\Psi}, \boldsymbol{V}) &= \ell(q - q_h, \boldsymbol{v} - \boldsymbol{v}_h) - A^N\left(p_h^{s,N}, \boldsymbol{u}_h^N; q - q_h, \boldsymbol{v} - \boldsymbol{v}_h\right) \\ &\quad + A^N\left(p_h^{s,N}, \boldsymbol{u}_h^N; q, \boldsymbol{v}\right) - A\left(p_h^{s,N}, \boldsymbol{u}_h^N; q, \boldsymbol{v}\right) \\ &= \ell(q - q_h, \boldsymbol{v} - \boldsymbol{v}_h) - A^N\left(p_h^{s,N}, \boldsymbol{u}_h^N; q - q_h, \boldsymbol{v} - \boldsymbol{v}_h\right) \\ &\quad + \langle(\mathscr{T} - \mathscr{T}_N)\, p_h^{s,N}, q\rangle_{\partial B_R} \\ &= \ell(q - q_h, \boldsymbol{v} - \boldsymbol{v}_h) - A^N\left(p_h^{s,N}, \boldsymbol{u}_h^N; q - q_h, \boldsymbol{v} - \boldsymbol{v}_h\right) \\ &\quad - \langle(\mathscr{T} - \mathscr{T}_N)\, \xi, q\rangle_{\partial B_R} + \langle(\mathscr{T} - \mathscr{T}_N)\, p^s, q\rangle_{\partial B_R}, \end{aligned}$$

which implies (21). □

We introduce the following four lemmas, which are used in the derivation of the a posterior error. For the sake of brevity, we have omitted the proof and provided the related literature for interested readers.

Lemma 7 (See [37]) *For any $p \in H^1(\Omega_a)$, we have*

$$\|p\|_{H^{1/2}(\partial B_R)} \lesssim \|p\|_{H^1(\Omega_a)}, \quad \|p\|_{H^{1/2}(\partial B_{R'})} \lesssim \|p\|_{H^1(\Omega_a)}.$$

Lemma 8 (See [37]) *Let $(p, \boldsymbol{u})$ be the solution to (9). We have*

$$\left|\hat{p}_n(R)\right| \lesssim \left(\frac{R'}{R}\right)^{|n|} |\hat{p}_n(R')|.$$

Lemma 9 (See [37]) *Let $\boldsymbol{\Phi} = (\gamma, \boldsymbol{w})$ be the solution to the dual problem (17). We have*

$$\left|\langle(\mathscr{T} - \mathscr{T}_N)\xi, \gamma\rangle_{\partial B_R}\right| \lesssim N^{-2}\|\xi\|^2_{H^1(\Omega_a)}.$$

Lemma 10 (See [16]) *Suppose that D has a Lipschitz boundary, and that p is a real number satisfying $1 \le p < \infty$. Then, there holds*

$$\|v\|_{L^p(\partial D)} \lesssim \|v\|^{1-1/p}_{L^p(D)} \|v\|^{1/p}_{W^1_p(D)}, \quad \forall v \in W^1_p(D).$$

In Lemma 9, it is shown that the truncation error of the DtN operator on the scattered field decay exponentially with respect to the truncation parameter N. Such a result implies that N can be small in practice. The following Lemma shows the estimate of (21).

Lemma 11 *For any $\boldsymbol{V} \in \mathcal{H}^1(\Omega)$, we have*

$$\begin{aligned}&\left|A(\boldsymbol{\Psi}, \boldsymbol{V}) + \langle(\mathscr{T} - \mathscr{T}_N)\xi, q\rangle_{\partial B_R}\right| \\ &\lesssim \left(\left(\sum_{K\in\mathcal{M}_{h,a}} \eta_{K,a}^2 + \sum_{K\in\mathcal{M}_{h,s}} \eta_{K,s}^2\right)^{1/2} + \left(\frac{R'}{R}\right)^N \left\|p^i\right\|_{H^2(\Omega_a)}\right) \|\boldsymbol{V}\|_{\mathcal{H}^1(\Omega)}.\end{aligned}$$

Proof Let

$$\begin{aligned}J_1 &= \ell(q - q_h, \boldsymbol{v} - \boldsymbol{v}_h) - A^N\left(p_h^{s,N}, \boldsymbol{u}_h^N; q - q_h, \boldsymbol{v} - \boldsymbol{v}_h\right), \\ J_2 &= \langle(\mathscr{T} - \mathscr{T}_N)p^s, q\rangle_{\partial B_R},\end{aligned}$$

where $(q_h, \boldsymbol{v}_h) \in \mathcal{H}_h^1(\Omega)$. It follows from (21) that

$$A(\boldsymbol{\Psi}, \boldsymbol{V}) + \langle(\mathscr{T} - \mathscr{T}_N)\xi, q\rangle_{\partial B_R} = J_1 + J_2.$$

By the definition of the sesquilinear form (14), we have

$$\begin{aligned}J_1 = &\sum_{K\in\mathcal{M}_{h,a}} \left(\int_K \left(-\nabla p_h^{s,N}\cdot\nabla(\overline{q} - \overline{q}_h) + \kappa^2 p_h^{s,N}(\overline{q} - \overline{q}_h)\right)\mathrm{d}\boldsymbol{x}\right. \\ &\left. + \sum_{e\in\partial_K\cap\Gamma}\int_e \left(\partial_{\boldsymbol{n}} p^i - \rho_f\omega^2\boldsymbol{u}_h^N\cdot\boldsymbol{n}\right)(\overline{q} - \overline{q}_h)\mathrm{d}s + \sum_{e\in\partial_K\cap\partial B_R}\int_e \mathscr{T}_N p_h^{s,N}(\overline{q} - \overline{q}_h)\mathrm{d}s\right) \\ &+ \sum_{K\in\mathcal{M}_{h,s}} \left(\int_K -\mathcal{E}_{\lambda,\mu}\left(\boldsymbol{u}_h^N, \boldsymbol{v} - \boldsymbol{v}_h\right) + \rho\omega^2\boldsymbol{u}_h^N\cdot(\overline{\boldsymbol{v}} - \overline{\boldsymbol{v}}_h)\mathrm{d}\boldsymbol{x} + \sum_{e\in\partial_K\cap\Gamma}\int_e -(p^i + p_h^{s,N})\boldsymbol{n}\cdot(\overline{\boldsymbol{v}} - \overline{\boldsymbol{v}}_h)\mathrm{d}s\right).\end{aligned}$$

Using the integration by parts, one can get

$$\begin{aligned}J_1 = &\sum_{K\in\mathcal{M}_{h,a}} \left(\int_K \left(\triangle p_h^{s,N} + \kappa^2 p_h^{s,N}\right)(\overline{q} - \overline{q}_h)\mathrm{d}\boldsymbol{x} - \sum_{e\in\partial_K}\int_e \nabla p_h^{s,N}\cdot\boldsymbol{\nu}(\overline{q} - \overline{q}_h)\mathrm{d}s\right. \\ &\left. + \sum_{e\in\partial_K\cap\Gamma}\int_e \left(\partial_{\boldsymbol{n}} p^i - \rho_f\omega^2\boldsymbol{u}_h^N\cdot\boldsymbol{n}\right)(\overline{q} - \overline{q}_h)\mathrm{d}s + \sum_{e\in\partial_K\cap\partial B_R}\int_e \mathscr{T}_N p_h^{s,N}(\overline{q} - \overline{q}_h)\mathrm{d}s\right) \\ &+ \sum_{K\in\mathcal{M}_{h,s}} \left(\int_K \left(\triangle^*\boldsymbol{u}_h^N + \rho\omega^2\boldsymbol{u}_h^N\right)\cdot(\overline{\boldsymbol{v}} - \overline{\boldsymbol{v}}_h)\mathrm{d}\boldsymbol{x} - \sum_{e\in\partial_K}\int_e \boldsymbol{T}\boldsymbol{u}_h^N\cdot(\overline{\boldsymbol{v}} - \overline{\boldsymbol{v}}_h)\mathrm{d}s\right. \\ &\left. + \sum_{e\in\partial_K\cap\Gamma}\int_e -(p^i + p_h^{s,N})\boldsymbol{n}\cdot(\overline{\boldsymbol{v}} - \overline{\boldsymbol{v}}_h)\mathrm{d}s\right) \\ = &\sum_{K\in\mathcal{M}_{h,a}} \left(\int_K \mathcal{R}_a p_h^{s,N}(\overline{q} - \overline{q}_h)\mathrm{d}\boldsymbol{x} + \sum_{e\in\partial_K}\frac{1}{2}\int_e J_{e,a}(\overline{q} - \overline{q}_h)\mathrm{d}s\right) \\ &+ \sum_{K\in\mathcal{M}_{h,s}} \left(\int_K \mathcal{R}_s\boldsymbol{u}_h^N\cdot(\overline{\boldsymbol{v}} - \overline{\boldsymbol{v}}_h)\mathrm{d}\boldsymbol{x} + \sum_{e\in\partial_K}\frac{1}{2}\int_e \boldsymbol{J_{e,s}}\cdot(\overline{\boldsymbol{v}} - \overline{\boldsymbol{v}}_h)\mathrm{d}s\right)\end{aligned}$$

Let $q_h = \Pi_h^a q$ and $\boldsymbol{v}_h = \Pi_h^s \boldsymbol{v}$, where Π_h^a and Π_h^s are the Scott-Zhang [47]and Clément [44] interpolation operators, respectively, with the following interpolation estimates

$$\|q - \Pi_h^a q\|_{L^2(K)} \lesssim h_K \|\nabla q\|_{L^2(\widetilde{K})}, \quad \|q - \Pi_h^a q\|_{L^2(e)} \lesssim h_e^{1/2} \|q\|_{H^1(\widetilde{K}_e)},$$

$$\|\boldsymbol{v} - \Pi_h^s \boldsymbol{v}\|_{L^2(K)} \lesssim h_K \|\nabla \boldsymbol{v}\|_{L^2(\widetilde{K})}, \quad \|\boldsymbol{v} - \Pi_h^s \boldsymbol{v}\|_{L^2(e)} \lesssim h_e^{1/2} \|\boldsymbol{v}\|_{H^1(\widetilde{K}_e)}.$$

Here, $\widetilde{K}$ and $\widetilde{K}_e$ are the union of all the elements in $\mathcal{M}_{h,s} \cup \mathcal{M}_{h,a}$, which have nonempty intersection with the element K and the side e, respectively. It follows from the Cauchy-Schwarz inequality and the above interpolation estimates that

$$\begin{aligned}
|J_1| \lesssim & \sum_{K \in \mathcal{M}_{h,a}} \left(h_K \left\| \mathcal{R}_a p_h^{s,N} \right\|_{L^2(K)} \|\nabla q\|_{L^2(\widetilde{K})} + \sum_{e \in \partial_K} \frac{1}{2} h_e^{1/2} \|J_{e,a}\|_{L^2(e)} \|q\|_{H^1(\widetilde{K}_e)} \right) \\
& + \sum_{K \in \mathcal{M}_{h,s}} \left(h_K \left\| \mathcal{R}_s \boldsymbol{u}_h^N \right\|_{L^2(K)} \|\nabla \boldsymbol{v}\|_{L^2(\widetilde{K})} + \sum_{e \in \partial_K} \frac{1}{2} h_e^{1/2} \|\boldsymbol{J_{e,s}}\|_{L^2(e)} \|\boldsymbol{v}\|_{H^1(\widetilde{K}_e)} \right) \\
\lesssim & \sum_{K \in \mathcal{M}_{h,a}} \left(h_K \left\| \mathcal{R}_a p_h^{s,N} \right\|_{L^2(K)} + \left(\sum_{e \in \partial_K} \frac{1}{2} h_e \|J_{e,a}\|_{L^2(e)}^2 \right)^{1/2} \right) \|q\|_{H^1(\Omega_a)} \\
& + \sum_{K \in \mathcal{M}_{h,s}} \left(h_K \left\| \mathcal{R}_s \boldsymbol{u}_h^N \right\|_{L^2(K)} + \left(\sum_{e \in \partial_K} \frac{1}{2} h_e \|\boldsymbol{J_{e,s}}\|_{L^2(e)}^2 \right)^{1/2} \right) \|\boldsymbol{v}\|_{H^1(\Omega_s)},
\end{aligned}$$

Using (15) and (16), we have

$$\begin{aligned}
|J_1| \lesssim & \left(\sum_{K \in \mathcal{M}_{h,a}} \eta_{K,a}^2 \right)^{1/2} \|q\|_{H^1(\Omega_a)} + \left(\sum_{K \in \mathcal{M}_{h,s}} \eta_{K,s}^2 \right)^{1/2} \|\boldsymbol{v}\|_{H^1(\Omega_s)} \\
\lesssim & \left(\sum_{K \in \mathcal{M}_{h,a}} \eta_{K,a}^2 + \sum_{K \in \mathcal{M}_{h,s}} \eta_{K,s}^2 \right)^{1/2} \|\boldsymbol{V}\|_{\mathcal{H}^1(\Omega)}.
\end{aligned}$$

The remain work is to estimate J_2. It follows from the definitions of (5) and (13) that

$$\begin{aligned}
|J_2| = |\langle (\mathscr{T} - \mathscr{T}_N) p^s, q \rangle_{\partial B_R}| &= \left| \frac{2\pi}{R} \sum_{|n| \geq N} h_n(\kappa R) \hat{p}_n^s(R) \overline{\hat{q}}_n(R) \right| \\
&\leq \left(\frac{2\pi}{R} \right) \sum_{|n| \geq N} |h_n(\kappa R)| |\hat{p}_n^s(R)| |\hat{q}_n(R)|.
\end{aligned}$$

Using Lemma 8, one can obtain

$$|J_2| \lesssim \sum_{|n|\geq N} 2\pi |h_n(\kappa R)| \left(\frac{R'}{R}\right)^{|n|} |\hat{p}_n^s(R')||\hat{q}_n(R)|$$
$$\lesssim \left(\frac{R'}{R}\right)^{N} \sum_{|n|\geq N} 2\pi |h_n(\kappa R)||\hat{p}_n^s(R')||\hat{q}_n(R)|.$$

It is shown in [23] that

$$|h_n(\kappa R)| \lesssim (1+n^2)^{1/2} \lesssim |n|, \tag{22}$$

which together with Lemma 7 yields

$$|J_2| \lesssim \left(\frac{R'}{R}\right)^{N} \left(\sum_{|n|\geq N} 2\pi(1+n^2)^{1/2}|\hat{p}_n^s(R')|^2\right)^{1/2} \left(\sum_{|n|\geq N} 2\pi(1+n^2)^{1/2}|\hat{q}_n(R')|^2\right)^{1/2}$$
$$\lesssim \left(\frac{R'}{R}\right)^{N} \|p^s\|_{H^{1/2}(\partial B_R')}\|q\|_{H^{1/2}(\partial B_R)} \lesssim \left(\frac{R'}{R}\right)^{N} \|p^s\|_{H^1(\Omega_a)}\|q\|_{H^1(\Omega_a)}.$$

Using the stability estimate (11), one can get

$$|J_2| \lesssim \left(\frac{R'}{R}\right)^{N} \|\boldsymbol{U}\|_{\mathcal{H}^1(\Omega)}\|\boldsymbol{V}\|_{\mathcal{H}^1(\Omega)}$$
$$\lesssim \left(\frac{R'}{R}\right)^{N} \left\|p^i\right\|_{H^2(\Omega_a)} \|\boldsymbol{V}\|_{\mathcal{H}^1(\Omega)}.$$

Combining the above estimates yields

$$|J_1 + J_2| \lesssim \left(\left(\sum_{K\in\mathcal{M}_{h,a}} \eta_{K,a}^2 + \sum_{K\in\mathcal{M}_{h,s}} \eta_{K,s}^2\right)^{1/2} + \left(\frac{R'}{R}\right)^{N} \left\|p^i\right\|_{H^2(\Omega_a)}\right) \|\boldsymbol{V}\|_{\mathcal{H}^1(\Omega)},$$

which completes the proof. □

We now give the main result.

Theorem 1 *Let $\boldsymbol{U}$ and $\boldsymbol{U}_{\boldsymbol{h}}^{\boldsymbol{N}}$ be the solutions of (9) and (14), respectively. Then, there exists a positive integer N_0 independent of h such that for any $N > N_0$, the following a posteriori error estimate holds*

$$\|\boldsymbol{U} - \boldsymbol{U}_{\boldsymbol{h}}^{\boldsymbol{N}}\|_{\mathcal{H}^1(\Omega)} \lesssim \left(\left(\sum_{K\in\mathcal{M}_{h,a}} \eta_{K,a}^2 + \sum_{K\in\mathcal{M}_{h,s}} \eta_{K,s}^2\right)^{1/2} + \left(\frac{R'}{R}\right)^{N} \left\|p^i\right\|_{H^2(\Omega_a)}\right).$$

Proof From (13) and (22), it is easy to verify that

$$Re\langle \mathscr{T}_N \xi, \xi\rangle_{\partial B_R} = 2\pi \sum_{|n|\le N} Re(h_n(\kappa R))|\hat{\xi}_n|^2 \le 0.$$

It follows from the Cauchy-Schwarz inequality and Lemma 10 that for any $\delta > 0$, there exists a positive constant $C(\delta)$ independent of N, such that

$$\begin{aligned}
|(a_3(\boldsymbol{\zeta}, \xi) + a_4(\xi, \boldsymbol{\zeta}))| &\lesssim \|\boldsymbol{\zeta}\|^2_{L^2(\Gamma)} + \|\xi\|^2_{L^2(\Gamma)} \\
&\lesssim \|\boldsymbol{\zeta}\|^2_{L^2(\Gamma)} + \|\xi\|^2_{L^2(\partial\Omega_a)} \\
&\lesssim \|\boldsymbol{\zeta}\|_{L^2(\Omega_s)}\|\boldsymbol{\zeta}\|_{H^1(\Omega_s)} + \|\xi\|_{L^2(\Omega_a)}\|\xi\|_{H^1(\Omega_a)} \\
&\lesssim C(\delta)\|\boldsymbol{\Psi}\|^2_{L^2(\Omega)} + \delta\|\boldsymbol{\Psi}\|^2_{\mathcal{H}^1(\Omega)}.
\end{aligned}$$

It follows from (20) and Lemma 11 that there exist three positive constants C_1, C_2 and C_3 independent of h and N such that

$$\begin{aligned}
\|\boldsymbol{\Psi}\|^2_{\mathcal{H}^1(\Omega)} \le & C_1 \left(\left(\sum_{K\in\mathcal{M}_{h,a}} \eta^2_{K,a} + \sum_{K\in\mathcal{M}_{h,s}} \eta^2_{K,s} \right)^{1/2} + \left(\frac{R'}{R}\right)^N \left\| p^i \right\|_{H^2(\Omega_a)} \right) \|\boldsymbol{\Psi}\|_{\mathcal{H}^1(\Omega)} \\
& + (C_2 + C(\delta))\|\boldsymbol{\Psi}\|^2_{L^2(\Omega)} + C_3\delta\|\boldsymbol{\Psi}\|^2_{\mathcal{H}^1(\Omega)}.
\end{aligned}$$

By (19), Lemma 9, Lemma 11 and (18), we have

$$\begin{aligned}
\|\boldsymbol{\Psi}\|^2_{L^2(\Omega)} \le & C_4 \left(\left(\sum_{K\in\mathcal{M}_{h,a}} \eta^2_{K,a} + \sum_{K\in\mathcal{M}_{h,s}} \eta^2_{K,s} \right)^{1/2} + \left(\frac{R'}{R}\right)^N \left\| p^i \right\|_{H^2(\Omega_a)} \right) \|\boldsymbol{\Psi}\|_{L^2(\Omega)} \\
& + C_5 N^{-2}\|\boldsymbol{\Psi}\|^2_{\mathcal{H}^1(\Omega)},
\end{aligned}$$

where $C_4 > 0$ and $C_5 > 0$ are independent of h and N. Combining the above two estimates, we have

$$\begin{aligned}
\|\boldsymbol{\Psi}\|^2_{\mathcal{H}^1(\Omega)} \le & (C_1 + C_4(C_2 + C(\delta))) \left(\left(\sum_{K\in\mathcal{M}_{h,a}} \eta^2_{K,a} + \sum_{K\in\mathcal{M}_{h,s}} \eta^2_{K,s} \right)^{1/2} + \left(\frac{R'}{R}\right)^N \left\| p^i \right\|_{H^2(\Omega_a)} \right) \|\boldsymbol{\Psi}\|_{\mathcal{H}^1(\Omega)} \\
& + \left((C(\delta) + C_2)\, C_5 N^{-2} + C_3\delta \right) \|\boldsymbol{\Psi}\|^2_{\mathcal{H}^1(\Omega)}.
\end{aligned}$$

Choose a sufficiently large integer N_0 such that $\left((C(\delta) + C_2)\, C_5 N^{-2} + C_3\delta \right) \le 1/2$, which completes the proof by taking $N > N_0$. □

5 Implementation and numerical examples

In this section, we discuss the algorithmic implementation of the adaptive DtN-FEM and present three numerical examples to demonstrate the effectiveness of the proposed method.

5.1 Adaptive algorithm

Based on the a posteriori error estimate from Theorem 1, we use the PDE toolbox of MATLAB to implement the adaptive algorithm of the linear finite element formulation. It is shown in Theorem 1 that the a posteriori error estimator consists of two parts: the finite element discretization error ϵ_h and the DtN truncation error ϵ_N, which depends on the truncation parameter N, where

$$\epsilon_h = \left(\sum_{K \in \mathcal{M}_{h,a}} \eta_{K,a}^2 + \sum_{K \in \mathcal{M}_{h,s}} \eta_{K,s}^2 \right)^{1/2}, \tag{23}$$

$$\epsilon_N = \left(\frac{R'}{R} \right)^N \left\| p^i \right\|_{H^2(\Omega_a)}. \tag{24}$$

In the implementation, we choose R', R and N based on (24) to make sure that the finite element discretization error is not polluted by the DtN truncation error, or more specifically, ϵ_N is required to be very small compared to ϵ_h, for example, $\epsilon_N \leq 10^{-8}$. For simplicity, in the following numerical experiments, R' is chosen such that the elastic solid is exactly contained in the circle $B_{R'}$, and N is taken to be the smallest positive integer such that $\epsilon_N \leq 10^{-8}$. The algorithm is shown in Algorithm 1 for the adaptive DtN-FEM to solve the acoustic-elastic interaction problem (9). In our numerical experiments, we always choose $\tau = 0.5$.

Algorithm 1 The adaptive DtN-FEM algorithm for the acoustic-elastic interaction problem.

1: Given the tolerance $\epsilon > 0$, $\tau \in (0, 1)$;
2: Fix the computational domain Ω by choosing the radius R;
3: Choose R' and N such that $\epsilon_N \leq 10^{-8}$;
4: Construct an initial triangulation $\mathcal{M}_h$ over Ω and compute error estimators;
5: **while** $\epsilon_h > \epsilon$ **do**
6: Refine the mesh $\mathcal{M}_h$ according to the strategy:
if $\eta_{\hat{T}} > \tau \max_{T \in \mathcal{M}_h} \eta_T$, then refine the element $\hat{T} \in \mathcal{M}_h$;
7: Denote the new mesh still by $\mathcal{M}_h$ and solve the discrete problem (14) on the new mesh $\mathcal{M}_h$;
8: Compute the corresponding error estimators;
9: **end while**

5.2 Numerical examples

We present three numerical examples to demonstrate the effectiveness of the proposed method. In the first example, the elastic body is a disk, where the corresponding problem has an analytical solution. In the second and third examples, the elastic bodies are square and U-shaped objects, respectively.

Example 1 We first introduce a model problem for which analytical solutions are available for the evaluation of accuracy; see [51]. Consider the scattering of a plane incident wave $p^i = e^{\mathrm{i}\kappa \boldsymbol{x}\cdot\boldsymbol{d}}$ with the propagation direction $\boldsymbol{d} = (1, 0)^\top$ by a disc-shaped elastic body of radius R_0. Denote the shear (or transverse) and the compressional (or longitudinal) elastic wave numbers by

$$\kappa_s = \omega\sqrt{\rho/\mu},$$
$$\kappa_p = \omega\sqrt{\rho/(\lambda + 2\mu)},$$

respectively. Thus, the analytical solutions of (3) can be written as

$$p^i(r,\theta) = \sum_{n=0}^{\infty} \epsilon_n \mathrm{i}^n J_n(\kappa r)\cos(n\theta),$$
$$p^s(r,\theta) = \sum_{n=0}^{\infty} A_n H_n^{(1)}(\kappa r)\cos(n\theta),$$
$$\boldsymbol{u} = \nabla\varphi + \nabla\times\psi,$$

with

$$\varphi(r,\theta) = \sum_{n=0}^{\infty} B_n J_n\left(\kappa_p r\right)\cos(n\theta),$$
$$\psi(r,\theta) = \sum_{n=0}^{\infty} C_n J_n\left(\kappa_s r\right)\sin(n\theta),$$

$$\epsilon_n = \begin{cases} 1 & \text{for } n = 0, \\ 2 & \text{for } n \neq 0. \end{cases}$$

where A_n, B_n, and C_n are to be determined. It follows from the the transmission conditions (1) and (2) that

$$\boldsymbol{E}_n \boldsymbol{X}_n = \boldsymbol{e}_n,$$

where $\boldsymbol{X}_n = (A_n, B_n, C_n)^\top$, $\boldsymbol{E}_n = \left[E_n^{ij}\right]$, and $\boldsymbol{e}_n = \left[e_n^j\right]$, $i, j = 1, 2, 3$. Their elements (identified by the super-script) are

$$
\begin{aligned}
E_n^{11} &= -H_{n-1}^{(1)}(\kappa R_0) + \frac{n}{\kappa R_0} H_n^{(1)}(\kappa R_0),\\
E_n^{12} &= \frac{\rho_f \omega^2 \kappa_p}{\kappa}\left[J_{n-1}\left(\kappa_p R_0\right) - \frac{n}{\kappa_p R_0} J_n\left(\kappa_p R_0\right)\right],\\
E_n^{13} &= \frac{\rho_f \omega^2 n}{\kappa R_0} J_n(\kappa_s R_0),\\
E_n^{21} &= 0,\\
E_n^{22} &= \frac{2\mu n \kappa_p}{R_0} J_{n-1}\left(\kappa_p R_0\right) - \frac{2\mu\left(n^2+n\right)}{R_0^2} J_n\left(\kappa_p R_0\right),\\
E_n^{23} &= \frac{2\mu\left(n^2+n\right) - \mu\kappa_s^2 R_0^2}{R_0^2} J_n(\kappa_s R_0) - \frac{2\mu\kappa_s}{R_0} J_{n-1}(\kappa_s R_0),\\
E_n^{31} &= H_n^{(1)}(\kappa R_0),\\
E_n^{32} &= \frac{2\mu\left(n^2+n\right) - \mu\kappa_s^2 R_0^2}{R_0^2} J_n\left(\kappa_p R_0\right) - \frac{2\mu\kappa_p}{R_0} J_{n-1}\left(\kappa_p R_0\right),\\
E_n^{33} &= \frac{2\mu n \kappa_s}{R_0} J_{n-1}(\kappa_s R_0) - \frac{2\mu\left(n^2+n\right)}{R_0^2} J_n(\kappa_s R_0),
\end{aligned}
$$

and

$$
\begin{aligned}
e_n^1 &= \epsilon_n \mathrm{i}^n \left[J_{n-1}(\kappa R_0) - \frac{n}{\kappa R_0} J_n(\kappa R_0)\right],\\
e_n^2 &= 0,\\
e_n^1 &= -\epsilon_n \mathrm{i}^n J_n(\kappa R_0).
\end{aligned}
$$

To ensure the accuracy of the analytic solution, we choose the first 21 terms for computation. We choose the parameters as $\omega = 1, \mu = 1, \lambda = 1, \rho = 1, \rho_f = 1, R_0 = 1$ and $R = 2$. In the implement of our adaptive DtN-FEM algorithm, we take $R' = 1$. It can be observed from Fig. 2 that the choice of the first 21 terms is reliable.

We firstly check the accuracy of the adaptive DtN-FEM. Figure 3 shows the magnitudes of the exact solutions and numerical solutions with $\kappa = 1$. One can observe that the numerical solutions are in a perfect agreement with the exact series solutions. Figure 4 shows the curves of $\log\epsilon_h$ and $\log e_h$ against $\log \mathrm{DoF}_h$ with $\kappa = 1, 2, 4$, respectively, where DoF_h denotes the number of nodal points of the mesh $\mathcal{M}_h$. It proves that the decays of the a priori and a posteriori errors are both $\mathcal{O}\left(\mathrm{DoF}_h^{-1/2}\right)$.

Example 2 Consider the scattering of the plane wave $p^i = e^{\mathrm{i}\kappa \boldsymbol{x}\cdot\boldsymbol{d}}$ with the propagation direction $\boldsymbol{d} = (1, 0)^\top$ by a square elastic body. Choose the parameters as $\omega = 1, \mu =$

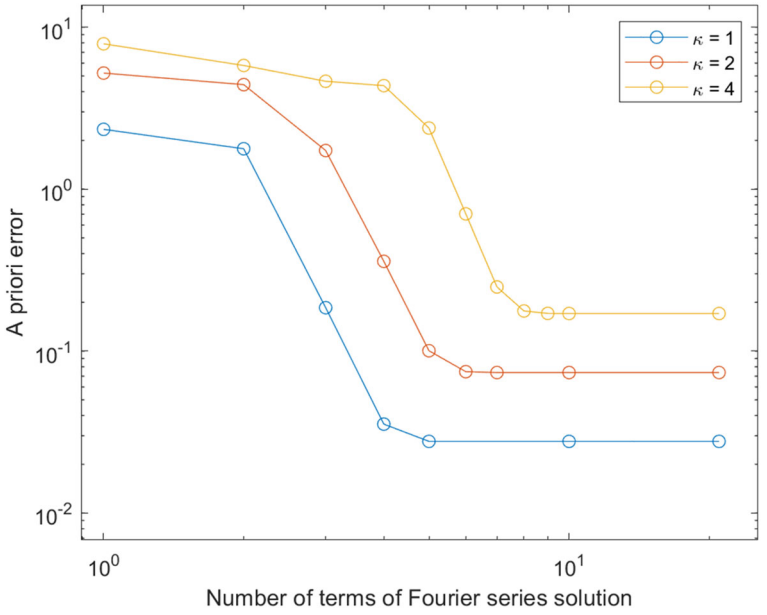

Fig. 2 Log-log plot for a priori errors versus the number of items of Fourier series solutions when the mesh size $h = 0.0269$

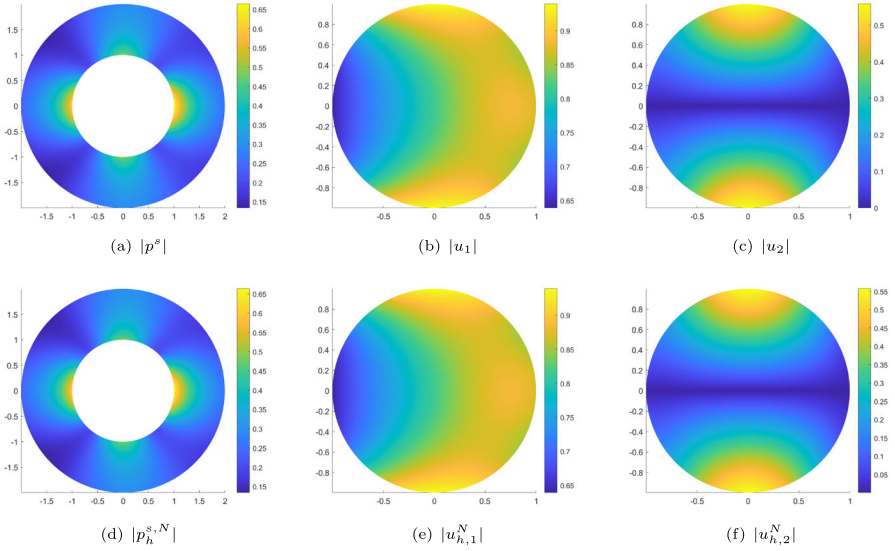

Fig. 3 Exact solutions (a,b,c) and numerical solutions (d,e,f) in Example 1

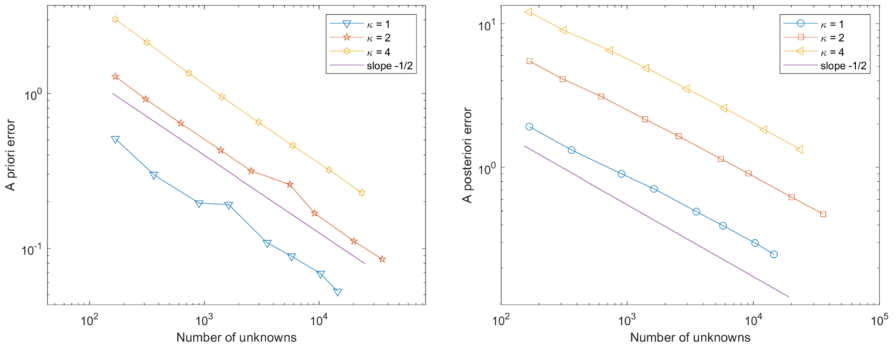

(a) A priori error (b) A posterior error

Fig. 4 Quasi-optimality of the a priori and a posteriori errors

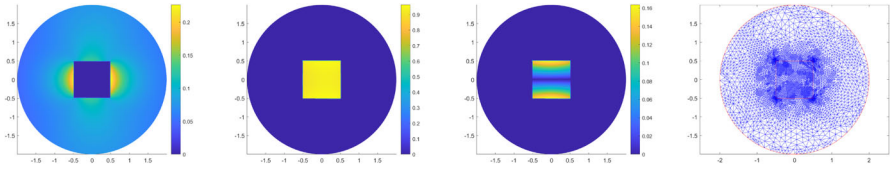

(a) $|p_h^{s,N}|$ (b) $|u_{h,1}^N|$ (c) $|u_{h,2}^N|$ (d) Adaptive mesh

Fig. 5 The magnitudes of the numerical solutions (a,b,c) with $\kappa = 1$ in Example 2; the adaptively refined mesh (d) with 10,569 elements after 10 refinement iterations

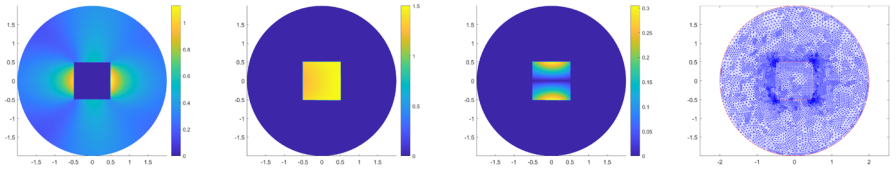

(a) $|p_h^{s,N}|$ (b) $|u_{h,1}^N|$ (c) $|u_{h,2}^N|$ (d) Adaptive mesh

Fig. 6 The magnitudes of the numerical solutions (a,b,c) with $\kappa = 2$ in Example 2; the adaptively refined mesh (d) with 14,365 elements after 10 refinement iterations

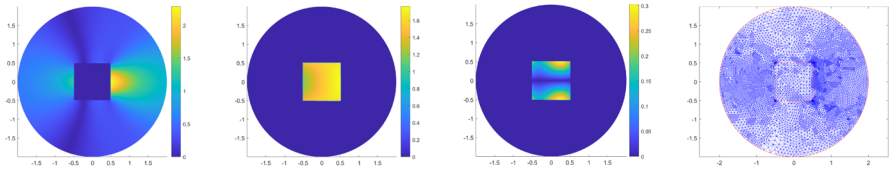

(a) $|p_h^{s,N}|$ (b) $|u_{h,1}^N|$ (c) $|u_{h,2}^N|$ (d) Adaptive mesh

Fig. 7 The magnitudes of the numerical solutions (a,b,c) with $\kappa = 4$ in Example 2; the adaptively refined mesh (d) with 12,475 elements after 6 refinement iterations

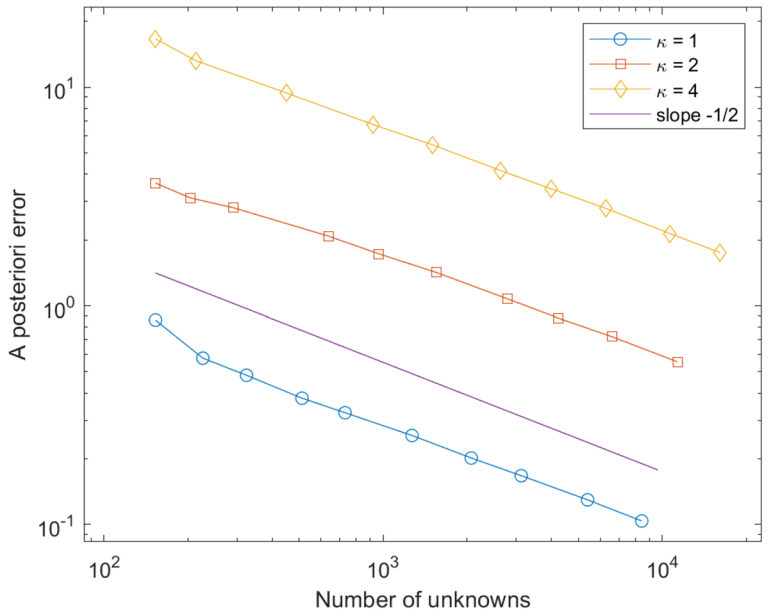

Fig. 8 Quasi-optimality of the a posteriori error estimates (right) with different κ in Example 2

Table 1 Comparison of numerical results using uniform and adaptive refinements with $\kappa = 1$ in Example 2

Uniform mesh			Adaptive mesh		
DoF_h	ϵ_h	Time (s)	DoF_h	ϵ_h	Time (s)
153	0.8605	0.0125	153	0.8605	0.0125
575	0.5389	0.0593	324	0.4820	0.1254
2229	0.3270	0.6393	730	0.3249	0.4240
8777	0.1949	6.9050	3123	0.1674	5.0985
34833	0.1165	106.1843	8439	0.1038	26.4549

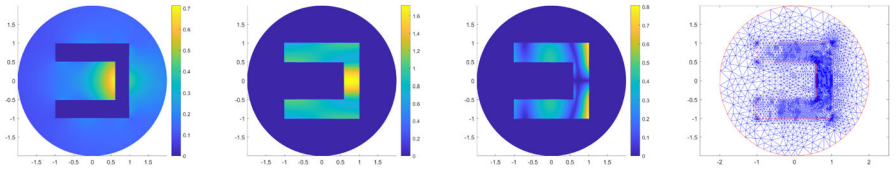

(a) $|p_h^{s,N}|$ (b) $|u_{h,1}^N|$ (c) $|u_{h,2}^N|$ (d) Adaptive mesh

Fig. 9 The magnitudes of the numerical solutions (a,b,c) with $\kappa = 1$ in Example 3; the adaptively refined mesh (d) with 10,123 elements after 10 refinement iterations

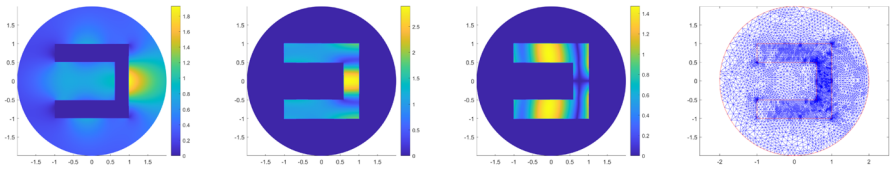

(a) $|p_h^{s,N}|$ (b) $|u_{h,1}^N|$ (c) $|u_{h,2}^N|$ (d) Adaptive mesh

Fig. 10 The magnitudes of the numerical solutions (a,b,c) with $\kappa = 2$ in Example 3; the adaptively refined mesh (d) with 12,349 elements after 10 refinement iterations

$1, \lambda = 1, \rho = 1, \rho_f = 1$ and $R = 2$. The side length of the square elastic solid is 1. In this example, we take $R' = 0.71$ in the implement of our adaptive algorithm. This example does not have an analytical solution and the solution contains singularity around the corners of the elastic solid.

Figures 5, 6 and 7 plot the magnitudes of the numerical solutions and the associated adaptive meshes with $\kappa = 1, 2, 4$, respectively. One can observe that the algorithm does capture the solution feature and adaptively refine the mesh around the corners of the elastic solid where the solution displays singularity. A comparison of a posteriori errors using the uniform and adaptive mesh refinements with $\kappa = 1$ is presented in Table 1. It can be observed that the adaptive mesh refinement requires fewer DoF_h and less cputime than the uniform mesh refinement to reach the close accuracy, which shows the advantage of using the adaptive mesh refinement. Figure 8 shows the curve of $\log\epsilon_h$ versus $\log \mathrm{DoF}_h$ with different wave number $\kappa = 1, 2, 4$. It proves that the decay of the a posteriori error estimates is $\mathcal{O}\left(\mathrm{DoF}_h^{-1/2}\right)$.

Example 3 Consider the scattering of the plane wave $p^i = e^{\mathrm{i}\kappa \boldsymbol{x}\cdot\boldsymbol{d}}$ with the propagation direction $\boldsymbol{d} = (1, 0)^\top$ by a U-shaped elastic body, where the elastic body is contained in $\{\boldsymbol{x} = (x_1, x_2)^\top \in \mathbb{R}^2 : -1 \leq x_1, x_2 \leqslant 1\}$. We set the parameters $\omega = 1, \mu = 1, \lambda = 1, \rho = 1$ and $\rho_f = 1$. This example also does not have an analytical solution and the solution contains singularity around the corners of the elastic solid. In this example, we take $R' = 1.43$.

Figures 9, 10 and 11 show the the magnitudes of the numerical solutions and the corresponding adaptive meshes with fixed $R = 2$ and different $\kappa = 1, 2, 4$, respectively. Again, the algorithm shows the capability of capturing the solution feature and adaptively refines the mesh around the corners of the solid. Table 2 shows the

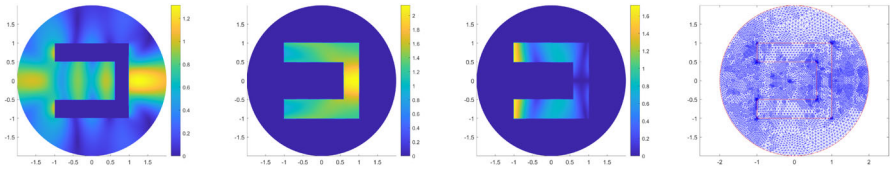

(a) $|p_h^{s,N}|$ (b) $|u_{h,1}^N|$ (c) $|u_{h,2}^N|$ (d) Adaptive mesh

Fig. 11 The magnitudes of the numerical solutions (a,b,c) with $\kappa = 4$ in Example 3; the adaptively refined mesh (d) with 14,308 elements after 6 refinement iterations

Table 2 Comparison of numerical results using uniform and adaptive refinements with $\kappa = 1$ in Example 3

Uniform mesh			Adaptive mesh		
DoF_h	ϵ_h	Time (s)	DoF_h	ϵ_h	Time (s)
163	19.6748	0.0139	163	19.6748	0.0139
675	4.3768	0.0688	266	3.3893	0.0971
2389	2.2203	0.7352	536	2.1135	0.2572
9417	1.2334	7.7851	1604	1.2323	1.5228
37393	0.7264	203.9922	5092	0.7263	9.0280

numerical results using adaptive and uniform refinements with $R = 2$ and $\kappa = 1$. Again, it shows the advantage of using adaptive mesh refinements. Figure 12 shows the curve of $\log\epsilon_h$ versus $\log \text{DoF}_h$ with the different truncated parameter N and radius R. The decay of the a posteriori error estimates is still $\mathcal{O}\left(\text{DoF}_h^{-1/2}\right)$, which proves that our adaptive DtN-FEM algorithm is robust with respect to the choice of the truncated parameter N and radius R.

6 Conclusion

In this paper, we present an adaptive finite element DtN method for the acoustic-elastic interaction problem. A new duality argument is developed to obtain the a posteriori error estimate. It does not only take into account of the finite element discretization error but also includes the truncation error of the DtN operator. We show that the truncation error decays exponentially with respect to the truncation parameter. The a posteriori error estimate for the solution of the discrete problem serves as a basis for the adaptive finite element approximation. Numerical results show that the proposed method is accurate and effective. This work provides a viable alternative to the adaptive finite element PML method for solving the acoustic-elastic interaction problem. It also enriches the range of choices available for solving wave propagation prob-

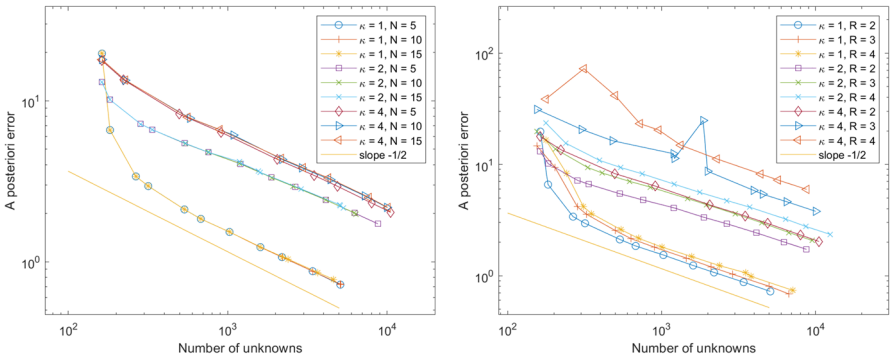

Fig. 12 Quasi-optimality of the a posteriori error estimates with different truncated parameter N (left) and radius R (right) in Example 3

lems imposed in unbounded domains. Future work includes extending our analysis to the adaptive DtN-FEM for solving the three-dimensional acoustic-elastic interaction problem, where a more complicated TBC needs to be considered. Besides, the implementation of adaptive algorithm for three-dimensional problems is significantly more complicated than for two-dimensional problems.

Acknowledgements This work of J.L. was partially supported by the National Natural Science Foundation of China grant 12271209 and Jilin Province Science and Technology Plan Development Project grant 20210201078GX.

Data Availability Statement All data generated or analysed during this study are included in this article.

Declarations

Conflict of Interest The authors declare no conflict of interest.

References

1. Arens, T.: The scattering of plane elastic waves by a one-dimensional periodic surface. Math. Methods Appl. Sci. **22**(1), 55–72 (1999)
2. Babuška, I., Aziz, A.: Survey lectures on mathematical foundations of the finite element method. In: Aziz, A. (ed.) The Mathematical Foundations of the Finite Element Method with Application to the Partial Differential Equations. Academic Press, New York (1973)
3. Babuška, I., Werner, C.: Error estimates for adaptive finite element computations. SIAM J. Numer. Anal. **15**, 736–754 (1978)
4. Bao, G., Gao, Y., Li, P.: Time-domain analysis of an acoustic-elastic interaction problem. Arch. Ration. Mech. Anal. **229**, 835–884 (2018)
5. Bao, G., Jiang, X., Li, P., Yuan, X.: An adaptive finite element DtN method for the elastic wave scattering by biperiodic structures. ESAIM Math. Model. Numer. Anal. **55**(6), 2921–2947 (2021)
6. Bao, G., Li, P., Lv, J.: Numerical solution of an inverse diffraction grating problem from phaseless data. J. Opt. Soc. Am. A **30**(3), 293–298 (2013)
7. Bao, G., Li, P., Wu, H.: An adaptive edge element method with perfectly matched absorbing layers for wave scattering by periodic structures. Math. Comp. **79**, 1–34 (2010)
8. Bao, G., Li, P., Yuan, X.: An adaptive finite element DtN method for the elastic wave scattering problem in three dimensions. SIAM J. Numer. Anal. **59**(6), 2900–2925 (2021)
9. Bao, G., Lin, Y.: Determination of random periodic structures in transverse magnetic polarization. Commun. Math. Res. **37**, 271–296 (2021)
10. Bao, G., Wu, H.: Convergence analysis of the perfectly matched layer problems for time harmonic Maxwell's s equations. SIAM J. Numer. Anal. **43**, 2121–2143 (2005)
11. Bao, G., Zhang, M., Hu, B., Li, P.: An adaptive finite element DtN method for the three-dimensional acoustic scattering problem. Discrete Contin. Dyn. Syst. Ser. B **26**(1), 61–79 (2021)
12. Bao, G., Zhang, M., Jiang, X., Li, P., Yuan, X.: An adaptive finite element DtN method for Maxwell's equations. East Asian J. Appl. Math. **13**, 610–645 (2023)
13. Bayliss, A., Turkel, E.: Radiation boundary conditions for numerical simulation of waves. Commun. Pure Appl. Math. **33**, 707–725 (1980)
14. Berenger, J.P.: A perfectly matched layer for the absorption of electromagnetic waves. J. Comput. Phys. **114**, 185–200 (1994)
15. Bramble, J.H., Pasciak, J.E., Trenev, D.: Analysis of a finite PML approximation to the three dimensional elastic wave scattering problem. Math. Comp. **79**, 2079–2101 (2010)
16. Brenner, S.C., Scott, L.R.: The Mathematical Theory of Finite Element Methods, 3rd edn. Springer, New York (2008)
17. Chen, J., Chen, Z.: An adaptive perfectly matched layer technique for 3-D time-harmonic electromagnetic scattering problems. Math. Comp. **77**, 673–698 (2008)

18. Chen, Z., Liu, X.: An adaptive perfectly matched layer technique for time-harmonic scattering problems. SIAM J. Numer. Anal. **43**, 645–671 (2005)
19. Chen, Z., Wu, H.: An adaptive finite element method with perfectly matched absorbing layers for the wave scattering by periodic structures. SIAM J. Numer. Anal. **41**, 799–826 (2003)
20. Chen, Z., Xiang, X., Zhang, X.: Convergence of the PML method for elastic wave scattering problems. Math. Comp. **85**, 2687–2714 (2016)
21. Chew, W., Weedon, W.: A 3D perfectly matched medium for modified Maxwell's equations with stretched coordinates. Microwave Opt. Technol. Lett. **13**, 599–604 (1994)
22. Engquist, B., Majda, A.: Absorbing boundary conditions for the numerical simulation of waves. Math. Comp. **31**, 629–651 (1977)
23. Ernst, O.G.: A finite-element capacitance matrix method for exterior Helmholtz problems. Numer. Math. **75**, 175–204 (1996)
24. Estorff, O.V., Antes, H.: On FEM-BEM coupling for fluid-structure interaction analyses in the time domain. Internat. J. Numer. Methods Engrg. **31**, 1151–1168 (1991)
25. Flemisch, B., Kaltenbacher, M., Wohlmuth, B.I.: Elasto-acoustic and acoustic-acoustic coupling on non-matching grids. Internat. J. Numer. Methods Engrg. **67**, 1791–1810 (2006)
26. Gächter, G.K., Grote, M.J.: Dirichlet-to-Neumann map for three-dimensional elastic waves. Wave Motion **37**, 293–311 (2003)
27. Gao, Y., Li, P., Zhang, B.: Analysis of transient acoustic-elastic interaction in an unbounded structure. SIAM J. Math. Anal. **49**(5), 3951–3972 (2017)
28. Grote, M., Keller, J.: On nonreflecting boundary conditions. J. Comput. Phys. **122**, 231–243 (1995)
29. Grote, M., Kirsch, C.: Dirichlet-to-Neumann boundary conditions for multiple scattering problems. J. Comput. Phys. **201**, 630–650 (2004)
30. Hagstrom, T.: Radiation boundary conditions for the numerical simulation of waves. Acta Numer. **8**, 47–106 (1999)
31. Hohage, T., Schmidt, F., Zschiedrich, L.: Solving time-harmonic scattering problems based on the pole condition. II: convergence of the PML method. SIAM J. Math. Anal. **35**, 547–560 (2003)
32. Hsiao, G.C.: On the boundary-field equation methods for fluid-structure interactions, In: Problems and Methods in Mathematical Physics (Chemnitz, 1993), vol. 134, Teubner-Texte Math., 79-88, Teubner, Stuttgart (1994)
33. Hsiao, G.C., Kleinman, R.E., Schuetz, L.S.: On variational formulations of boundary value problems for acoustic-elastic interactions. In: Elastic Wave Propagation (Galway, 1988), vol. 35. North-Holland Ser. Appl. Math. Mech. North-Holland, Amsterdam (1989)
34. Hsiao, G.C., Nigam, N., Pasciak, J.E., Xu, L.: Error analysis of the DtN-FEM for the scattering problem in acoustics via Fourier analysis. J. Comput. Appl. Math. **235**, 4949–4965 (2011)
35. Hsiao, G.C., Sanchez-Vizuet, T., Sayas, F.-J.: Boundary and coupled boundary-finite element methods for transient wave-structure interaction. IMA J. Numer. Anal. **37**, 237–265 (2017)
36. Jiang, X., Li, P., Zheng, W.: Numerical solution of acoustic scattering by an adaptive DtN finite element method. Commun. Comput. Phys. **13**, 1277–1244 (2013)
37. Jiang, X., Li, P., Lv, J., Zheng, W.: An adaptive finite element method for the wave scattering with transparent boundary condition. J. Sci. Comput. **72**, 936–956 (2017)
38. Jiang, X., Li, P.: An adaptive finite element PML method for the acoustic-elastic interaction in three dimensions. Commun. Comput. Phys. **22**, 1486–1507 (2017)
39. Jiang, X., Li, P., Lv, J., Zheng, W.: An adaptive finite element PML method for the elastic wave scattering problem in periodic structures. ESAIM Math. Model. Numer. Anal. **51**, 2017–2047 (2017)
40. Jiang, X., Li, P., Lv, J., Zheng, W.: Convergence of the PML solution for elastic wave scattering by biperiodic structures. Commun. Math. Sci. **16**, 985–1014 (2018)
41. Jiang, X., Li, P., Lv, J., Wang, Z., Wu, H., Zheng, W.: An adaptive finite element DtN method for Maxwell's equations in biperiodic structures. IMA J. Numer. Anal. **42**(3), 2794–2828 (2022)
42. Jones, D.S.: Low-frequency scattering by a body in lubricated contact. Q. J. Mech. Appl. Math. **36**, 111–137 (1983)
43. Li, P., Yuan, X.: Convergence of an adaptive finite element DtN method for the elastic wave scattering by periodic structures. Comput. Methods Appl. Mech. Engrg. **360**, 112722 (2020)
44. Li, P., Yuan, X.: An adaptive finite element DtN method for the elastic wave scattering problem. Numer. Math. **150**(4), 993–1033 (2022)
45. Li, Y., Zheng, W., Zhu, X.: A CIP-FEM for high frequency scattering problem with the truncated DtN boundary condition. CSIAM Trans. Appl. Math. **1**, 530–560 (2020)

46. Luke, C.J., Martin, P.A.: Fluid-solid interaction: acoustic scattering by a smooth elastic obstacle. SIAM J. Appl. Math. **55**, 904–922 (1995)
47. Scott, L.R., Zhang, S.: Finite element interpolation of nonsmooth functions satisfying boundary conditions. Math. Comp. **54**, 483–493 (1990)
48. Soares, D., Mansur, W.: Dynamic analysis of fluid-soil-structure interaction problems by the boundary element method. J. Comput. Phys. **219**, 498–512 (2006)
49. Wang, Z., Bao, G., Li, J., Li, P., Wu, H.: An adaptive finite element method for the diffraction grating problem with transparent boundary condition. SIAM J. Numer. Anal. **53**, 1585–1607 (2015)
50. Xu, L., Yin, T.: Analysis of the Fourier series Dirichlet-to-Neumann boundary condition of the Helmholtz equation and its application to finite element methods. Numer. Math. **147**(4), 967–996 (2021)
51. Yin, T., Hsiao, G.C., Xu, L.: Boundary integral equation methods for the two dimensional fluid-solid interaction problem. SIAM J. Numer. Anal. **55**, 2361–2393 (2017)
52. Yuan, X., Bao, G., Li, P.: An adaptive finite element DtN method for the open cavity scattering problems. CSIAM Trans. Appl. Math. **1**, 316–345 (2020)
53. Yue, J., Li, P., Yuan, X., Zhu, X.: A diffraction problem for the biharmonic wave equation in one-dimensional periodic structures. Results Appl. Math. 100350 (2023)
54. Zhang, M., Lv, J.: Numerical method of profile reconstruction for a periodic transmission problem from single-sided data. Commun. Comput. Phys. **24**(2), 435–453 (2018)